Broadening of rectified potential structures induced by rf currents in a magnetized plasma: Application to ITER scrape-off-layer

E. Faudot,[1] L. Colas,[2] S. Heuraux,[1] and J. P. Gunn[2]
[1]*IJL, Nancy Universite, 54500 Vandoeuvre les Nancy, France*
[2]*IRFM, CEA, F-13108 Saint-Paul-lez-Durance, France*

(Received 16 November 2009; accepted 17 February 2010; published online 8 April 2010)

Measurements show that the vicinity of powered ion cyclotron range of frequency (ICRF) antennae is biased positively with respect to its environment [J. Gunn *et al.*, Proc. 22nd IAEA Fusion Energy Conference, Geneva 2008, EX/P6-32]. This is attributed to radio-frequency (rf) sheath rectification. The radial penetration of these direct current (dc) potentials from ICRF launchers into the tokamak scrape-off layer (SOL) determines the power deposition on the walls and especially on the antenna structure, which is a key point for long time clean discharges. Within independent flux tube models of rf sheath rectification the radial penetration of dc potentials is determined by the skin depth $x_0 = c/\omega_{pe}$ for the slow wave. When self-consistent exchange of transverse rf current is allowed between neighboring flux tubes, such a structure can be broadened radially up to a characteristic transverse length L. Broadening arises as soon as $L > x_0$. A linear modeling of the process gives a first evaluation of the theoretical length $L=(L_{\|}\rho_{ci}/2)^{1/2}$. Within the "flute assumption," it scales with the length $L_{\|}$ of open flux tubes and the ion Larmor radius Ω_{ci}. This trend has been confirmed by nonlinear fluid simulations using the SEM code taking into account nonlinearities of the sheath dynamics. Parametric regimes are outlined where broadening or nonlinearity arise. Langmuir probe measurements on Tore Supra suggest that the observed broadening is lower than predicted by the code. This suggests that actual rf current exchanges probably do not occur over the whole length of magnetic field lines but only on a fraction of it. This "effective parallel magnetic connection length" $L_{\|}^{\mathrm{eff}}$ is estimated from the measurements. The model is finally applied to several potential maps generated by an ITER antenna, with different plasma parameters depending on possible SOL scenarios in ITER, and "reasonable assumptions" about $L_{\|}^{\mathrm{eff}}$. It comes out that L ranges between 1 and 10 cm depending on local $L_{\|}^{\mathrm{eff}}$ and on typical ITER plasma parameters. © *2010 American Institute of Physics*. [doi:10.1063/1.3357334]

I. INTRODUCTION

This work is involved in a more general study concerning the spatial modifications induced by radio-frequency (rf) phenomena in the scrape-off layer (SOL) of tokamaks[1] but it can be generalized to all rf magnetized plasmas. rf phenomena are induced by rf waves radiated by ion cyclotron range of frequency (ICRF) antennas embedded in the outer wall of tokamaks. It can also be rf voltages driven by a cathode in a magnetron discharge. This work was motivated by the observation of hot spots in the corner of ICRF antennas in Tore Supra and other tokamaks. These hot spots are high localized heat loads[2] involving spurious and deleterious effects such as fusing and vaporization of the wall's material. These heat loads are generated by high energy beams composed of ions accelerated in high direct current (dc) potential structures around antennae during a shot. Indeed, this biasing results from the rectification of rf potential by sheaths localized at the end of open magnetic lines in front of ICRF antennae. The typical corresponding configuration appears between bumpers protecting the antenna structure. Each magnetic line intercepted by bumpers can be seen as a flux tube along which the potential oscillate at rf frequency and is longitudinally constant. This is equivalent to a double probe model. Concerned rf potentials are calculated from the integration of the parallel electric field mainly induced by the slow wave radiated by the antenna.[3]

rf rectification was first studied by Godyak.[4] This phenomenon results from the nonlinear V-I characteristic of a sheath due to the great difference between electron and ion mass. Consequently, the space charge in the sheath stays positive while the plasma density is high enough to screen the rf potential applied on the wall. Then, the plasma potential is always higher than the wall potential, the negative rf potentials are thus rectified and the dc flux tube is biased to highly positive dc potentials. Other sheaths models were developed by Liebermann[5,6] who refined the dc biasing and other sheath parameters from the influence of parallel polarization currents and sheath capacitance. However, in the frame of the problem described above, a model has been developed to take into account the effect of transverse (perpendicular to the magnetic field) rf currents on the rectification. The temporal study demonstrated analytically and numerically that the biasing is increased[7] by rf transverse currents, which are driven by transverse potential gradients themselves generated by inhomogeneities of antenna structure (i.e., box, Faraday screen,…). The dc potential structures are then equal and even higher than $2\phi_{\mathrm{rf}}/\pi$ and can theoretically reach $\phi_{\mathrm{rf}}/2$. This result is close to those Liebermann obtained only with a parallel sheath dynamics.

These potentials penetrate radially into the edge plasma such as an evanescent wave (the slow wave) characterized by a less than centimetric skin depth. This penetration length

has already been diagnosed by rf current measurements in the SOL of Tokamak Experiment for Technology Oriented Research (TEXTOR).[8] These results show that the radial penetration is centimetric. Other measurements with a reciprocating probe have been done on Tore Supra and give the potential distribution around an ICRF antenna.[9] In the same way, the penetration is centimetric but no more.

The way radial structures will be modified by transverse rf currents has not yet been investigated theoretically. Reference 10 already defines a radial length L_x from a vorticity model in which the potential is a streamfunction for the convection.[11] In these models, only amplitude of rf currents and potentials are taken into account and not rf temporal variations. This paper is therefore a complement of Ref. 7 because it described the spatial broadening of dc potential structures, which could explain separatrix polarization suspected in Joint European Torus (JET) rf.[11]

The first part repeats the analytical context already described in Ref. 7 and then shows how the theoretical length L characterizing the limit broadening can be approached by a linearized model. Next this is confirmed by a numerical modeling and a two-dimensional (2D) fluid code able to handle the nonlinear behavior of the equations. The predictions of the code are confronted to Langmuir probe measurements around a powered Tore Supra ICRF antenna. This work will permit to evaluate if dc potential structures can drastically disturb plasma convection until the separatrix or not. Thus it is a key issue to prevent or evaluate high heat loads on and around antenna structure.[12] The final purpose is obviously to make long pulse discharge possible in ITER by minimizing all heat sources able to damage materials and to create impurities in the plasma core. That is why the last part is dedicated to simulations of realistic ITER scenarios with the electric fields expected in front of ITER ICRF antennas.

II. RF SHEATH PHYSICS

The following model takes into account the rectification of rf potential by sheath dynamics and includes rf transverse currents equivalent to polarization currents.[13] Potentials and currents are calculated self-consistently along a flux tube, a tube of plasma ended by two sheaths along a constant magnetic field. The geometry is sketched in Fig. 1. The effect of intense ICRF near fields on the SOL surrounding the wave launcher is modeled as a pure rf potential difference ϕ_{rf} induced between both ends of each open flux tube. The nonlinear reaction of the plasma is a rectification of this pure rf drive into enhanced dc sheath potentials. Since the drive ϕ_{rf} is spatially inhomogeneous a differential biasing of nearby flux tube is expected. Correlatively transverse currents are likely to flow due to the plasma transverse conductivity. The present model solves self-consistently the biasing and the current circulation in two dimensions transverse to the confinement magnetic field.

The model has been deduced supposing that the parallel conductivity is much higher than perpendicular conductivity so that no longitudinal potential structures can grow. In a magnetized plasma, the electrostatic dispersion relation is $k_\perp/k_\parallel = \pm\sqrt{\epsilon_\parallel/\epsilon_\perp}$ (Ref. 14) and parallel modes cannot arise

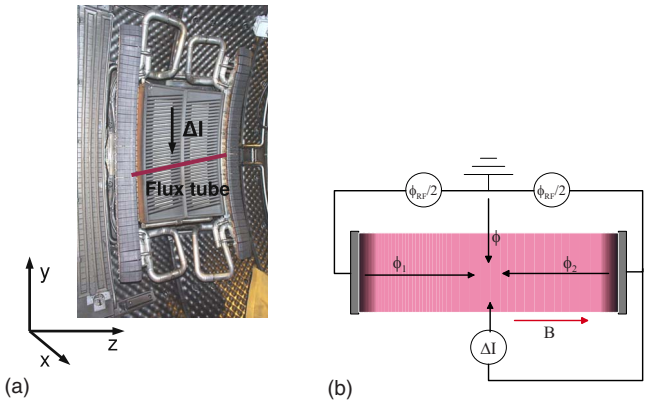

FIG. 1. (Color online) The physical device representing the ICRF antenna in Tore Supra appears in (a) and the model device representing a flux tube is schematized as an electric double probe model in (b).

while $k_\parallel < 1/L_\parallel$, which means $|L_\parallel^2/\epsilon_\parallel| < |L_\perp^2/\epsilon_\perp|$ with $k_\perp = 1/L_\perp$. In typical fusion plasmas, the absolute value of $\epsilon_\perp = 1-\omega_{pi}^2/(\omega^2-\Omega_{ci}^2)$ is much lower than the absolute value of $\epsilon_\parallel = 1-\omega_{pe}^2/\omega^2$, and the last inequality is verified, while $L_\parallel$ is not so higher than $L_\perp$. For instance, with typical deuterium plasma parameters in the SOL, $f \approx f_{ci}$, $n \approx 10^{18}$ m^{-3}, $B = 3$ T and $L_\perp = 10^{-2}$ m,[7] and $|L_\perp^2/\epsilon_\perp| = 1.16\ 10^{-5}$. Then, $L_\parallel$ should be smaller than 56 cm to verify the inequality. It comes out that as soon as $L_\parallel$ is higher than 56 cm the flute hypothesis is not valid, modes can develop and then the model has to be modified, for example by considering an effective length for the flux tube instead of the real length equal to the magnetic connection length. This will be discussed in Sec. V.

In the same way, the sheath width Δ has to be taken into account: the parallel rf electric field is screened from the plasma and appears only in the sheath when $\Lambda = -\epsilon_\parallel \Delta/L_\parallel \gg 1$.[15] In typical edge fusion plasmas, this parameter is higher than 1 with $f \approx f_{ci}$, $L \approx 1$ m, and $n \approx 10^{18}$ m^{-3}.

Under both these conditions ($|L_\parallel^2/\epsilon_\parallel| \ll |L_\perp^2/\epsilon_\perp|$ and $\Lambda \gg 1$) the flute hypothesis can be applied along the flux tube.

(1) The electron density distribution follows the Boltzmann law.
(2) The mass of electrons is neglected compared with the mass of ions.
(3) rf currents are the biggest contribution to perpendicular currents. Conduction current due to collision, convective current (equivalent to inertia current in Ref. 16 or "polarization" current in Ref. 17) due to transverse speed shear have been neglected for such structures. Collisions are too weak and convective currents become comparable to rf currents only for very small structures (1 mm).[17,7] Typical structures here are centimetric
(4) The plasma density in front of antenna is constant.
(5) The magnetic field is constant.

According to these hypotheses, the solving of the parallel current conservation equation without transverse currents gives Eq. (1),

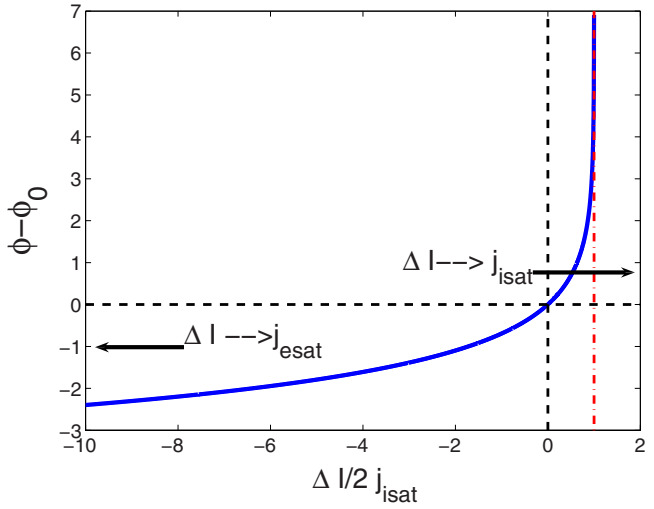

FIG. 2. (Color online) V-I characteristic of the double probe model. j_{isat} is the ion saturation current and j_{esat} is the electron saturation current 3.

$$\phi_0 = \phi_{fl} + \log\left[\cosh\left(\frac{\phi_{\mathrm{rf}}}{2}\right)\right]. \tag{1}$$

This equation is the rf rectified potential[4] including the floating potential $\phi_{fl}=e\cdot V_{fl}/T_e$ and rf potential $\phi_{\mathrm{rf}}=e\cdot V_{\mathrm{rf}}/T_e$ with T_e the electron temperature in eV

$$V_{\mathrm{rf}} = \int_{L_\parallel} E_\parallel dl. \tag{2}$$

V_{rf} is the rf potential resulting from the integration of the parallel electric field along open magnetic lines in front of antenna [Eq. (2)]. $L_\parallel$ is the parallel magnetic connection length. To take into account transverse currents, the quantity $\Delta I_\perp$ is added in the following set of equations:

$$\frac{\Delta I_\perp}{2j_{\mathrm{isat}}} = 1 - \exp(\phi_0 - \phi), \tag{3}$$

$$\frac{1}{\Omega_{ci}^2}\frac{\partial^2}{\partial t^2}\left(\frac{\Delta I_\perp}{2j_{\mathrm{isat}}}\right) + \frac{\Delta I_\perp}{2j_{\mathrm{isat}}} = \frac{L_\parallel \rho_{ci}}{2\Omega_{ci}}\left(\nu_i + \frac{\partial}{\partial t}\right)\Delta_\perp \phi. \tag{4}$$

Equation (3) is the current conservation in which $\Delta I_\perp$ is the current influx perpendicular to the flux tube and the LHS term is the parallel current driven by both sheaths. ϕ is the instantaneous local plasma potential with respect to a ground plane. Since the proposed model is electrostatic the notion of "ground" (strictly valid for dc potentials) is still meaningful at rf frequencies. Figure 1 shows how the grounding was chosen symmetric with respect to the left and right walls. j_{isat} is the ion saturation current. Figure 2 illustrates Eq. (3).

Equation (4) is deduced by deriving the momentum equation for ions[7] and is valid for frequencies lower and higher than Ω_{ci}. The same equation for electrons is neglected because their mass makes the electron current very weak. ρ_{ci} is the ion Larmor radius, Ω_{ci} is the ion cyclotron angular frequency, and ν_i is the ion-neutral collision frequency. The time derivative of the LHS term is the polarization current induced by the time variation in the rf electric fields. The resistive current term appears through ν_i and other terms have been neglected as supposed at the beginning of this section.

Then, the solving of current conservation 3 and momentum equation (4) along a double probe model gives Eq. (5). Equation (5) is strongly nonlinear that is why it can only be solved numerically

$$\left(\frac{1}{\Omega_{ci}^2}\frac{\partial^2}{\partial t^2}(\phi-\phi_0) - \frac{1}{\Omega_{ci}^2}\left[\frac{\partial}{\partial t}(\phi-\phi_0)\right]^2 - 1\right)\exp(\phi_0-\phi)+1 = \frac{L_\parallel \rho_{ci}}{2\Omega_{ci}}\left(\nu_i + \frac{\partial}{\partial t}\right)\Delta_\perp \phi. \tag{5}$$

Equation (5) solves the rectified potential ϕ in a plane perpendicular to the magnetic field in front of ICRF antenna. Then both the spatial behavior of the rectified potential and the temporal behavior can be studied. By averaging the rectified potential ϕ over one period, one obtains the dc rectified potential ϕ_{dc} used to compute convective cells resulting from $\mathbf{E}\times\mathbf{B}$ drifts in front of antenna.[18]

In the absence of transverse rf currents (i.e., within an independent flux tube approach), $\phi(x,t)=\phi_0(x,t)$ decays radially over a characteristic length x_0 of the order of the plasma skin depth. In the framework of the model outlined above, we would like to investigate how far the dc potentials ϕ_{dc} extend radially when self-consistent transverse exchanges of rf currents are allowed. First it is shown that the linearized version of the problem exhibits the characteristics of a (generalized) diffusion equation in the radial direction. A characteristic diffusion length $L(\omega)$ is determined from the parameters of the problem. Broadening arises as soon as $L(\omega)>x_0$. Then nonlinear simulations show that rf solicitations at frequency ω can drive dc potentials spanning over a length of the order of $L(\omega)$. On a typical Tore Supra discharge this length is finally compared with that inferred from Langmuir probe measurements.

III. LINEAR ANALYSIS

A. Linear modeling

The original systems 3 and 4 are nonlinear due to the parallel dynamics of sheath. Far from sheath saturation the system can be linearized supposing that $|\phi(x,t)-\phi_0(x,t)| \ll 1$, whatever t or equivalently $|\Delta I_\perp(x,t)| \ll 2j_{\mathrm{isat}}$. Each frequency harmonic being independent the time variation can be supposed sinusoidal with a characteristic pulsation ω. This gives Eqs. (6) and (7) on which Sec. IV will be based. Here the model is applied to a one-dimensional (1D) geometry to simplify the study of the broadening

$$\phi(x,\omega) - L^2(\omega)\Delta\phi(x,\omega) = \phi_0(x,\omega) \Leftrightarrow \phi(x,\omega) - \Delta I_\perp = \phi_0(x,\omega), \tag{6}$$

$$L^2(\omega) = L_{\mathrm{coll}}^2 + L_{\mathrm{nocoll}}^2 = \frac{L_\parallel^{\mathrm{eff}}\rho_{ci}}{2}\left[\frac{\nu_i}{\Omega_{ci}} + i\frac{\omega/\Omega_{ci}}{1-\omega^2/\Omega_{ci}^2}\right]. \tag{7}$$

$L(\omega)$ depends on the parallel length of the flux tube $L_\parallel$, the ion Larmor radius ρ_{ci}, the ion cyclotron Ω_{ci}, and rf angular frequencies ω. At zero frequency, the noncollisional term of

Eq. (7) vanishes. This formula remains valid, while $L^2\Delta\phi(x)$ is close to 0, which means that in a first approximation $\phi(x)\approx\phi_0(x)$. The spatial shape of the rf potential is supposed to be exponential such as the slow wave in magnetic plasmas[3] $\phi_{\rm rf}(x)=\phi_{\rm rf}\exp(-x/x_0)$ with x_0 the characteristic skin depth equivalent to the radial width of the potential structure in front of an ICRF antenna.

The following part will consist in evaluating a criterion of linearity for the present model. Equation (1) can be rewritten supposing that $\phi_{\rm rf}\gg\phi_{fl}$ as follows:

$$\phi_0(x,t)=\phi_{fl}+\ln\left\{\cosh\left[\frac{\phi_{\rm rf}}{2}\exp\left(-\frac{x}{x_0}\right)\cos(\omega t)\right]\right\}$$
$$\approx\frac{\phi_{\rm rf}}{2}\exp\left(-\frac{x}{x_0}\right)|\cos(\omega t)|, \tag{8}$$

with

$$|\cos(\omega t)|=\frac{2}{\pi}\left(1-2\sum_{n=1}^{\infty}\frac{(-1)^n}{4n^2-1}\cos(2n\omega t)\right). \tag{9}$$

1. Weak broadening

Here a weak broadening means that the radial shape of the potential structure is weakly modified by transverse current flow. This is the case when the length L is smaller than the structure width x_0: $L^2/x_0^2<1$

Equation (4) becomes at low frequency ($\omega<\Omega_{ci}$)

$$\Delta I_\perp(x,t)=\frac{L_\parallel\rho_{ci}}{2\Omega_{ci}}\frac{\partial^3}{\partial t\,\partial x^2}\phi(x,t). \tag{10}$$

Moreover, at high frequency ($\omega>\Omega_{ci}$)

$$\Delta I_\perp(x,t)=\frac{L_\parallel\rho_{ci}\Omega_{ci}}{2}\frac{\partial^2}{\partial x^2}\int_0^{T/2}\phi(x,t). \tag{11}$$

The low frequency criterion of linearity is then

$$\Delta I_\perp(x,t)=\frac{\phi_{\rm rf}}{2}\frac{L_{\rm LF}^2}{x_0^2}\,\mathrm{sign}[\cos(\phi)]\sin(\omega t)\ll 1, \tag{12}$$

with $L_{\rm LF}^2=L_\parallel\rho_{ci}\omega/\Omega_{ci}$. This criterion can then be simply written as follows:

$$\phi_{\rm rf}<\frac{x_0^2}{L_{\rm LF}^2}, \tag{13}$$

and the high frequency criterion of linearity in the interval $\omega t\in[-\pi/2;\pi/2]$

$$\Delta I_\perp(x,t)=\frac{\phi_{\rm rf}}{2}\frac{L_{\rm HF}^2}{x_0^2}\left(\frac{2\omega t}{\pi}-\sin(\omega t)\right)\ll 1, \tag{14}$$

with $L_{\rm HF}^2=L_\parallel\rho_{ci}\Omega_{ci}/\omega$. Considering that $\max[2\omega t/\pi-\sin(\omega t)]\to 9.52$, this criterion can be written as follows:

$$\phi_{\rm rf}<9.52\frac{x_0^2}{L_{\rm HF}^2}. \tag{15}$$

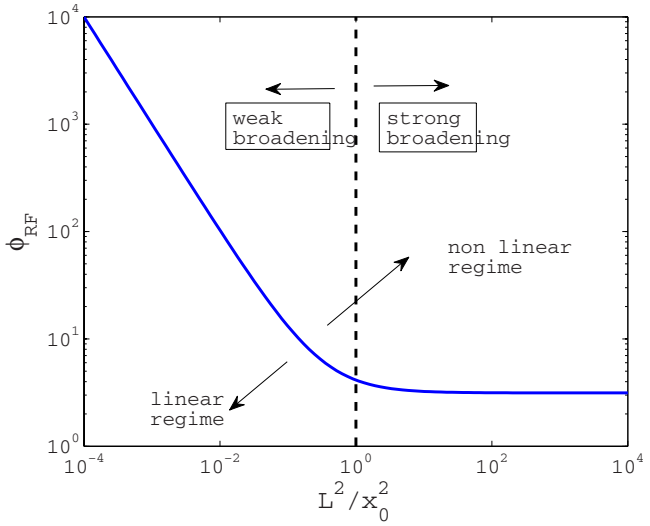

FIG. 3. (Color online) Parametric diagram of the four regimes involved in the modeling described by Eq. (5): linear with weak broadening, linear with strong broadening, nonlinear weak broadening, and nonlinear strong broadening. The broadening of the potential structure $\phi(x)$ depends on the parameter L^2/x_0^2 and the linear/nonlinear boundary corresponds to Eq. (18).

2. Strong broadening

A strong broadening means that the potential structure is widely modified by transverse currents. This is the case when the length L is higher or equal to the structure width x_0: $L^2/x_0^2>1$.

The criterion corresponding to a strong broadening and valid for all frequencies can be written as follows supposing that a strongly rectified structure equals the dc structure at each time step. Since the term L^2/x_0^2 is much higher than 1, it limits the temporal amplitude of the oscillating part of $\phi(x,t)$ because the expression $L^2/x_0^2\phi(x,t)$ cannot exceed 1 [see Eq. (3)]. This corresponds to transverse currents equal to twice the ion saturation current ($\Delta I_\perp=2j_{\rm isat}$). Then $\phi(x,t)$ is equal to its dc component: $\phi(x,t)\to\phi_{rf}/\pi$ and from Eq. (6) one can write $\Delta I_\perp$

$$\Delta I_\perp(x,t)=\phi_{\rm rf}\left(\frac{1}{\pi}-\frac{1}{2}|\cos(\omega t)|\right)<1. \tag{16}$$

The last equation gives simply the strong broadening criterion at all frequencies

$$\phi_{\rm rf}<\pi. \tag{17}$$

3. Four sheath regimes

The union of the weak and strong broadening criteria of linearity corresponding to the condition $\Delta I_\perp<1$ gives a global criterion

$$\phi_{\rm rf}<\left(\pi+\frac{x_0^2}{L^2}\right). \tag{18}$$

Figure 3 illustrates these four regimes governing the rectification of rf potential structures.

B. Solving the linear broadening

Equation (6) is either a diffusion equation when L is real or a wave equation if L^2 is real negative (L pure imaginary). In typical edge tokamak plasmas collisions can be ignored so that L^2 is pure imaginary. The system will depend on this parameter L compared with the original size of the potential structure $\phi_0(x)$. The typical spatial shape of $\phi_0(x)$ is a decreasing exponential because it describes the evanescence of the slow wave in a magnetized plasma. Then the source term is defined in Eq. (19)

$$\phi_0(x) = \phi_0 \exp(-|x|/x_0), \tag{19}$$

with x_0 the decreasing length of the potential structure, this length is actually a skin depth. Then Eq. (6) becomes Eq. (20),

$$\phi(x) - L^2 \Delta \phi(x) = \phi_0 \exp(-|x|/x_0). \tag{20}$$

Moreover, the solution is given by the convolution of $\phi_0(x)$ and a Green function $G(x)$

$$\phi(x) = \int_{-\infty}^{+\infty} \phi_0(x') G(x-x') dx'. \tag{21}$$

The Green function can be obtained with a Fourier transform and is defined in Eq. (22)

$$G(x) = -\frac{1}{2L} \exp\left(-\frac{|x|}{L}\right). \tag{22}$$

This solution has been reduced to $-(1/2L)\exp(-|x|/L)$ supposing that $\phi(+\infty)=\phi(-\infty)=0$.

The general solution of Eq. (21) appears in Eq. (23),

$$\phi(x) = \frac{\phi_0}{x_0^2 - L^2}\left[-L(\omega)^2 \exp\left(-\frac{|x|}{L}\right) + x_0^2 \exp\left(-\frac{|x|}{x_0}\right)\right]. \tag{23}$$

Expression (23) gives the shape of the structure depending on two decreasing lengths x_0 and L. Then the first order equivalent length for $\phi(x)$ as defined in Eq. (23) is simply

$$L_{\mathrm{eq}} = \frac{(x_0^2 - L^2)x_0 L}{x_0^2 L - L^2 x_0} = x_0 + L, \tag{24}$$

L can be complex, which means that the solution $\phi(x)$ can oscillate along x with the wave number $k=\Im(1/L)$ and in the meantime exponentially decreases with the characteristic length $1/\Re(1/L)$. The pertinent length defining the broadening is explicitly the inverse of the real part of $1/L(\omega)$.

By setting $L=a+ib$, different regimes taking into account real and imaginary parts can be deduced. Equation (23) becomes

$$\frac{\phi(x)}{\phi_0} = \left(\frac{1}{x_0^2 - L^2}\right)\left[x_0^2 \exp\left(-\frac{|x|}{x_0}\right) - L^2 \exp\left(-\frac{a-ib}{\|L\|^2}|x|\right)\right], \tag{25}$$

three regimes are possible: if $a>b$ the solution is aperiodic, so that spatial oscillations of the potential are negligible. Only a fraction of the period is visible over the length L. If $a>b$ the solution is pseudoperiodic, several oscillations can be observed over the length L. This result can be verified in Fig. 4.

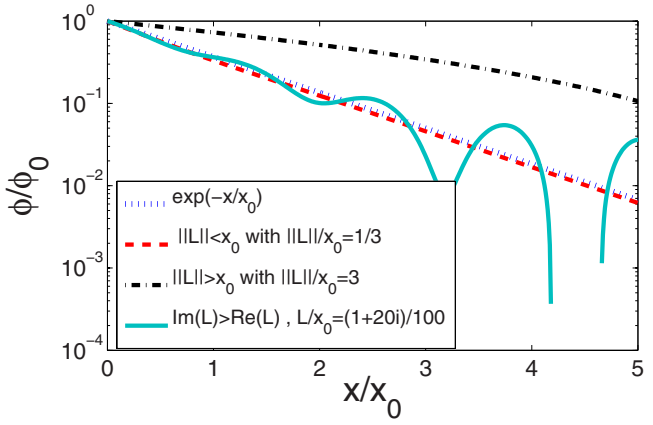

FIG. 4. (Color online) Decreasing profile of a potential structure penetrating in a plasma as a function of x for realistic values of L.

In the present case, $L^2=i\lambda^2$ is pure imaginary and then $a=b=\lambda/\sqrt{2}$. Then, Eq. (25) can be written as follows:

$$\frac{\phi(x)}{\phi_0} = \left(\frac{1}{x_0^2 - L^2}\right)\left\{x_0^2 \exp\left(-\frac{|x|}{x_0}\right) - L^2 \exp\left[\frac{(i-1)|x|}{\lambda\sqrt{2}}\right]\right\}. \tag{26}$$

For $x_0 \gg \lambda\sqrt{2}$, the width L can be neglected and $\phi(x)$ can be reduced as follows:

$$\phi(x) \approx \phi_0(x) = \phi_0 \exp(-|x|/x_0). \tag{27}$$

The potential structure remains unchanged, the solution is directly given by the source term.

For $x_0 \ll \lambda\sqrt{2}$

$$\phi(x) \approx \phi_0 \exp[-|x|/L(\omega)]. \tag{28}$$

In that case, the potential structure is broadened because the main contribution $\phi(x)$ comes from $\exp(-|x|/\sqrt{2}\lambda)$, the solution takes the Green function's shape.

Figure 4 summarizes the behavior of Eq. (26)–(28). The spatial effect of transverse currents is to broaden the initial rf potential structure to a size defined by L.

IV. NONLINEAR ANALYSIS

The linear equation for the potential appears in Eq. (6). The initial nonlinear Eq. (3) cannot be treated analytically but previous analysis of dc rectified Gaussian potential have shown that nonlinear effects mainly peaked the top part of the structure and meanwhile do not broaden the structure (see our last paper[7]). Actually, it has been shown that the rectification ratio $\phi_{\mathrm{dc}}/\phi_{\mathrm{rf}}$ depends on the parameter $\omega\tau_\perp\phi_{\mathrm{rf}}/2$ with $\tau_\perp = 4L_\parallel\rho_{ci}/2\Omega_{ci}r_0^2$ with r_0 the width of the potential Gaussian structure. When this parameter $\omega\tau_\perp\phi_{\mathrm{rf}}/2$ is higher than 1, which means for a high rf potential, the rectification ratio can reach 1/2, while this ratio is close to $1/\pi$ for low potentials. Thus the higher part of the structure tends to be peaked compared with the lower part. This nonlinear effect tends to decrease the broadening of a normalized structure. Simulations in Sec. V confirm quantitatively this effect.

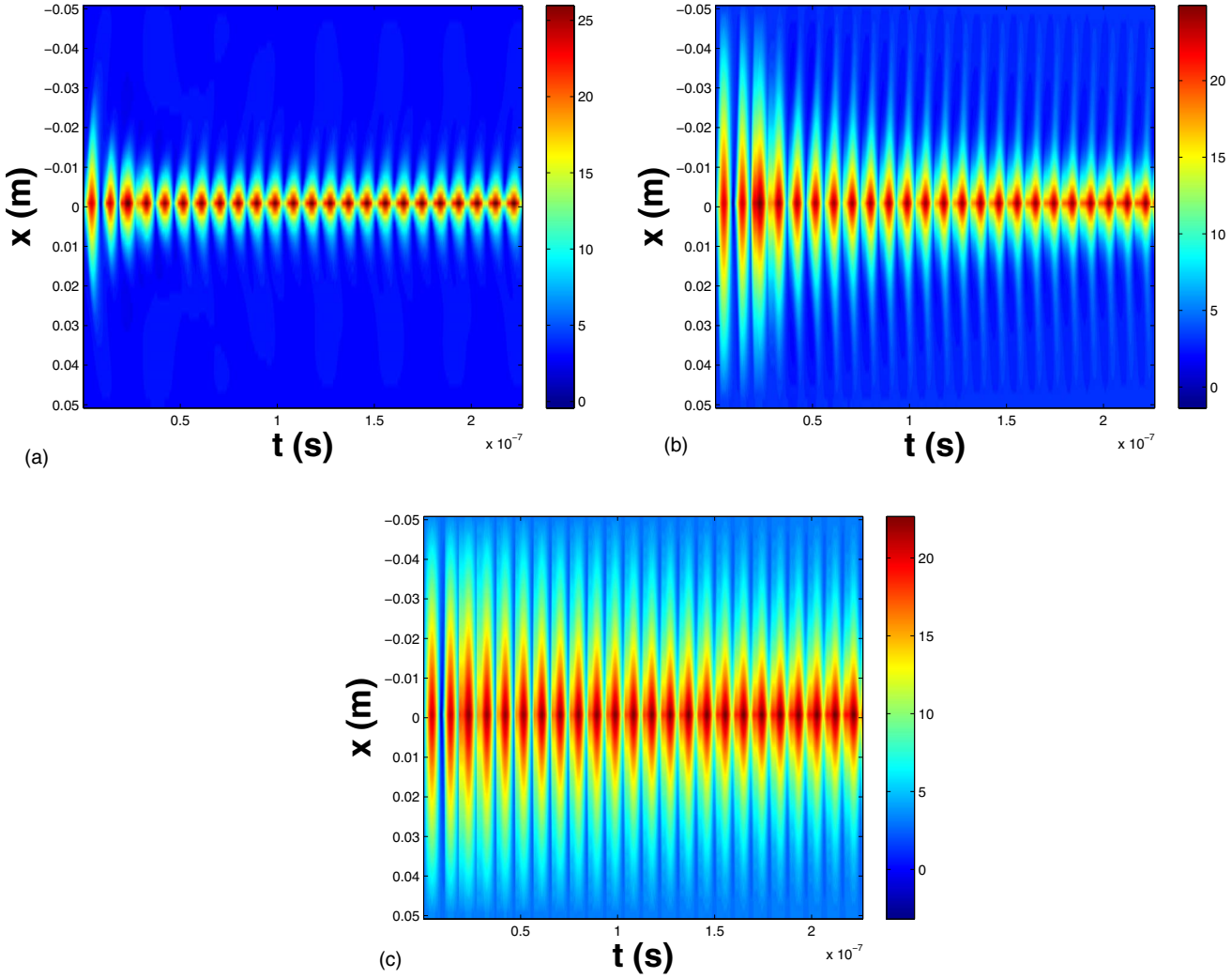

FIG. 5. (Color online) Comparison of the decreasing length of the rf rectified potential $\phi(x,t)$ as defined in Eq. (5) for three values of $L^2(\omega)$ by making vary $L_{\|}$=0.3, 3, and 30 m the magnetic line length or the flux tube length.

A. Nonlinear broadening computed by SEM code

Linear modeling provides insight into the broadening process. Yet in a linear approach, all time harmonics are decoupled, so that a solicitation at the rf wave frequency ω does not modify the dc potential. As long as the dc transverse plasma conductivity is null, inhomogeneous dc solicitations produce no transverse dc current, i.e., no broadening either. Numerical computations allow accessing the nonlinear domain whereby inhomogeneous rf solicitations are able to broaden the dc potentials.

The aim of the 2D fluid code sheath effect modeling (SEM) is to simulate self-consistently the rectified potential induced by rf sheath taking into account transverse rf current.[19] A finite difference method is implemented to solve the system described by Eq. (5) over a grid that can be defined by users. Here the 2D code has been simplified to a 1D code to reduce calculation time.

The input profile for the rf solicitation is a decreasing exponential function along x (radial coordinate in a Tokamak geometry), which matches the near field profile radiated by the ICRF antenna with a skin depth x_0. The shape of the source term in such a geometry is given by Eq. (19).

The total length of the simulated profile is 20 cm, which is long enough to simulate a realistic edge plasma between the antenna Faraday screen and the separatrix. A set of simulations have been run by varying ϕ_{rf} from 10 to 150 and $L_{\|}$ from 1 to 30 m. These parameters are chosen so that they cover the whole range of magnetized plasma parameters expected in tokamak SOL. It describes typical potential structures expected in Tore Supra for the same typical plasma conditions (magnetic field, density, deuterium plasma, temperature and frequency). The working frequency is 53 MHz and the ion cyclotron frequency is 32 MHz for a deuterium plasma. The choice to work with dimensional values is justified by the fact that all results can be easily compared with the effective values observed or expected in tokamaks.

Three samples of the resulting (x,t) potential maps are represented in Figs. 5(a)–5(c) and show the transient phase during which the width of the structure decreases until it reaches a stationary value. These (x,t) map are time averaged over the last simulated period to obtain the normalized (maximum amplitude=1) potential profile along x whose three samples appear in Figs. 6(a)–6(c). The floating potential has been removed from the potential profile. These fig-

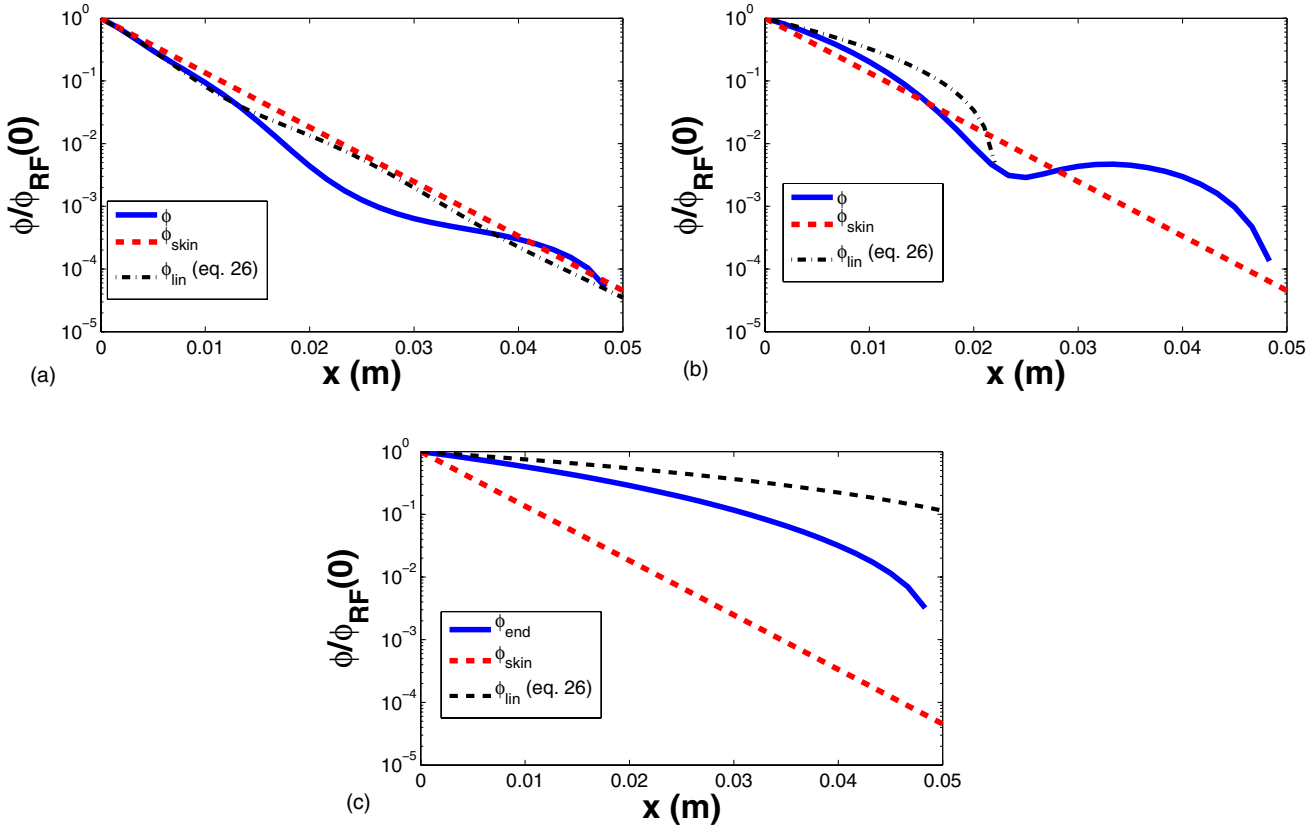

FIG. 6. (Color online) dc rectified potential profile ϕ normalized to its maximum value as a function of x. This profile is compared with the rf potential profile ϕ_0 and the theoretical linear potential profile ϕ_{lin} for three values of $L(\omega)$ corresponding to [(a)–(c)]. This profile results from the average of the potential map $\phi(x,y,t)$ along y.

ures permit to compare the nonlinear width L_{nl} [Eq. (29)] resulting from the simulation to the width L defined in Eq. (30) and to x_0 the skin depth of the slow wave.

The width L_{nl} is mathematically deduced from between $x=0$ and $x=x_0$

$$L_{nl} = \frac{x_0}{\ln \phi(0) - \ln \phi(x_0)}. \tag{29}$$

L_{nl} is based on the slope of the potential structure along x, then we lose the information about the amplitude of the potential structures. By drawing the "true" potential profiles, one can observe that the time averaged rectified potential profile $\phi(x)$ at $x=0$ is always below $\phi_{\text{rf}}(x)/2$ and always higher than ϕ_{rf}/π the dc value for the nonrectified rf potential.[7]

Moreover, L is the theoretical broadening length for a pure noncollisional plasma deduced from Eq. (7)

$$L = \sqrt{\frac{L_{\|}\rho_{ci}}{2}}\left[i\frac{\omega_0/\Omega_{ci}}{1-\omega_0^2/\Omega_{ci}^2}\right]. \tag{30}$$

It can be seen in Figs. 6(a)–6(c) that ϕ_{lin} calculated with Eq. (25) matches $\phi(x)$ the nonlinear potential profile computed by the code. The slight differences between them may come from the boundary condition set to 0 in the simulation instead of V_{fl} in Eq. (25). It clearly appears in these figures that $\phi(x)$, $\phi_{\text{lin}}(x)$, and $\phi_{\text{skin}} \equiv \phi_0(x)$ are quite close, while $\|L\|$ is smaller than x_0. As soon as $\|L\|$ is higher than x_0, the structure is broadened such as in Fig. 6(c). For high $\|L\|/x_0$, L_{nl} stays shorter than the width predicted by the linear theory. Then, the nonlinear effects occurring in the code make decrease the width of the normalized potential profile. It is important to keep in mind that potentials are normalized, which means that the potential shape is divided by the maximum amplitude of the shape. The true dc rectified potential shape $\phi(x)$ is always higher than $\phi_0(x)$ but the normalized $\phi(x)$ can exhibit a smaller width L than the normalized $\phi_0(x)$. This comes from the contraction induced by the normalization.

The combination of all simulations permits to build a surface for L_{nl} as a function of L and ϕ_{rf} the rf potential applied in simulations. The contour of isocurves is drawn to produce two new figures representing L_{nl}, respectively, as a function of L [Fig. 7(a)] and ϕ_{rf} [Fig. 7(b)].

In Fig. 7(a), $L_{\|}$ varies from 1 m to 30 m. For low values of L, the L_{nl} curve is linear with a slope of the order of x_0+L. When ϕ_{rf} increases L_{nl} curves seem to saturate down to a value which is much smaller than x_0+L. This means the more nonlinear the system is, the less the normalized structure is broadened. Moreover, the other important result is that L_{nl} curve is always below L_0 curve defined in Eq. (31), while $\phi_{\text{rf}} > 20$, which means for high potential values

$$L_0 = x_0 + \sqrt{\frac{L_{\|}\rho_{ci}}{2}}. \tag{31}$$

L_0 can be obtained from Eq. (24) simply by ignoring the frequency term of Eq. (30).

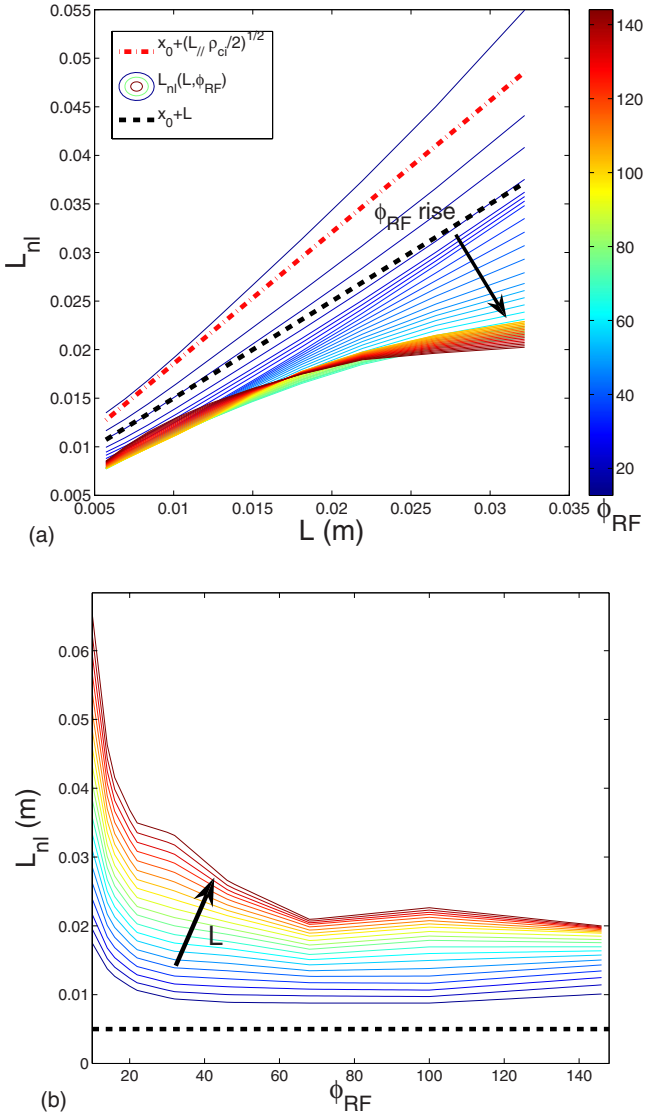

FIG. 7. (Color online) [(a) and (b)] Variation in the computed width L_{nl} as a function of two parameters L. (a) The linear broadening length and ϕ_{rf}. (b) The rf potential resulting from integration of the parallel electric field. L_{nl} is compared with L and x_0 is the skin depth for parallel electric field.

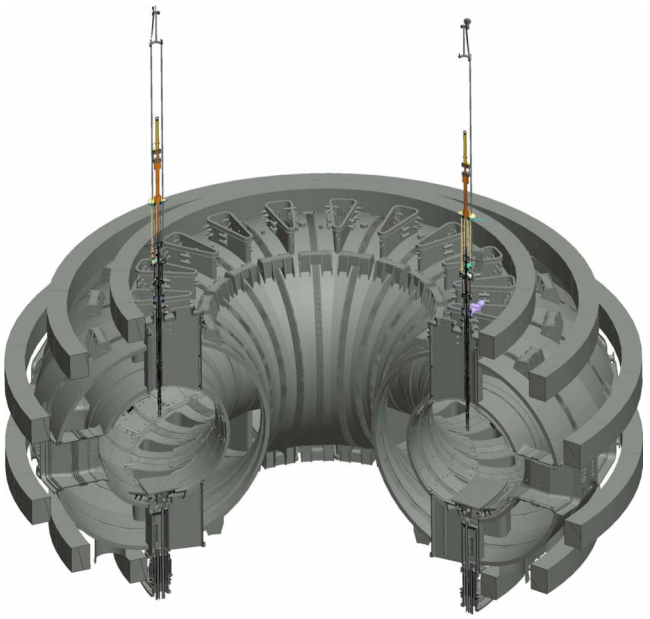

FIG. 8. (Color online) Sketch of the reciprocating probe mechanism plunging from the upper part of the tokamak chamber into the plasma.

In the same way x_0+L seems to fit the average of L_{nl} curves for different ϕ_{rf}, which means that the linear resolution of the model approximates the average behavior of the nonlinear model except for high value of L. In addition, Fig. 7(b) gives the variation in L as a function of $\phi_{rf}(0)$. For small values of $\phi_{rf}(0)$, L_{nl} curve shows an important broadening which becomes smaller and smaller when ϕ_{rf} increases.

The code does not permit to explore a range of ϕ_0 higher than 150 because nonlinearities make the simulation crash. Moreover the more the system is nonlinear the longer is the simulation time to make the structure converge. For high potential simulations ($\phi_0>100$) the simulation time should probably be increased to reach a consistent convergence.

V. MAGNETIC CONNECTION LENGTH

The previous linearized modeling revealed the existence of four broadening regimes (see Fig. 3). The broadening of potential structures appears as soon as $L>x_0$, but L depends on the square root of $L_{\|}$ the length of the magnetic lines. In tokamaks and especially in big machines, this length can be very long up to 10 or 20 m. In such cases L is much higher than x_0 and then the broadening of radial structure should be much large. For example, for a typical shot in Tore Supra with $x_0=5$ mm, $L_{\|}=1$, $B=3$ T, $n=10^{18}$ m^{-3}, and $f=57$ MHz, the broadening given by L is equal to 2 cm. If $L_{\|}=10$ m, then the broadening reaches more than 6 cm. This value has then to be compared with experimental measurements to be validated or on the contrary to modify the modeling. Some recent measurements with a reciprocating Langmuir probe pointed out that the broadening is smaller than expected by the model.

The reciprocating probe plunges into the plasma quasiradially (see Fig. 8, the angle between probe penetration axis and the radial direction can be neglected). One side of the probe is connected to the ICRF antenna and the other side to the limiter. While the probe side connected to the limiter does not see any spatial potential variation, the probe side connected to the ICRF antenna exhibits a peaked radial dc potential profile characteristic of the rectified potential in front of antenna (see Fig. 9). The radial width of the profile gives an approximation of the radial broadening which seems to stay smaller than the width resulting from the SEM code with a realistic magnetic length. This leads to think that transverse rf currents might be only exchanged over a fraction of magnetic connection length, which means an effective parallel length $L_{\|}^{\text{eff}}$.

From the radial potential profile, this effective magnetic length can be deduced considering our linear modeling which links the parallel length of the flux tube and the perpendicular width $L_{\perp}$ (equivalent to L) of the potential structure [Eq. (32)]. According to Tore Supra parameters (see beginning of this section) and the potential profile measured by the reciprocating probe which is 1.2 cm width, this length should be equal to 0.35 m. This is widely smaller than the 7

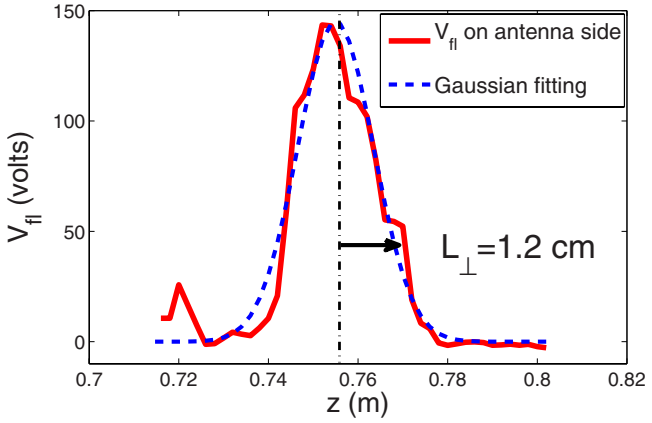

FIG. 9. (Color online) Floating potential profile obtained with a reciprocating probe penetrating straightforward into the plasma SOL along a quasiradial direction and crossing the magnetic lines connected to the ICRF antenna on Tore Supra.

m of the real connection length which is the distance between the probe and the antenna. Thus this $L_{\parallel}^{\text{eff}}=0.35$ m could be used to simulate specific Tore Supra scenarios

$$L_{\parallel}^{\text{eff}} = 2\frac{(L_{\perp}-x_0)^2}{\rho_{ci}}. \tag{32}$$

In a larger machinelike ITER, magnetic connection length in the SOL should be still longer (between 20 and 30 m). Considering such lengths, $L_{\perp}$ should be as larger as 10 cm. This length has been confirmed by SEM code simulation with $L_{\parallel}=28$ m. Nevertheless, one could expect that, like in Tore Supra, the perpendicular broadening is limited to few centimeters according to the effective magnetic length. It appears clearly in the discussion of Sec. II concerning the assumption of the model that the flute hypothesis is not systematically valid in edge fusion plasmas. It has been shown that the hypothesis is no more valid as soon as $L_{\parallel}$ is higher than 56 cm for one centimeter radial structures, which is of the same order than $L_{\parallel}^{\text{eff}}=35$ cm deduced from probe measurements. The matching of $L_{\parallel}^{\text{eff}}$ found from probe measurements and from a 2D electrostatic modeling[14] should be estimated from many shots to be validated. For the moment this has been done only for one shot.

From Tore Supra data one could expect the same centimetric radial structures in ITER. This kind of results has already been observed on TEXTOR, which is a smaller tokamak. In TEXTOR, the radial potential profile still exhibits 2–3 cm wide structures for much shorter magnetic connection length and other parameters closed to Tore Supra's ones ($T_e=10-30$ eV, $n_e=2.10^{19}$ m^{-3}, and $B=2.25$ T).[8] Then the width of potential structures seems to be less dependant on the magnetic connection length than on other parameters as the wavelength of the electrostatic modes (in a first approximation) able to arise along the toroidal magnetic field. The same calculation as in Sec. II can be achieved with ITER parameters: $T_e=20$ eV, $n_e=10^{19}$ m^{-3}, $B=4$ T, and $f\approx 50$ MHz. In that case, $L_{\parallel}^{\text{eff}}$ approaches 1.6 m still with $L_{\perp}=1$ cm. However, one needs $L_{\perp}$ to deduce $L_{\parallel}^{\text{eff}}$ or the contrary. Then a good evaluation can only come from a self-consistent modeling taking into account longitudinal and perpendicular modes in the flux tube cavity as well as sheath rectification. For the moment one can just say that in big machine $L_{\parallel}^{\text{eff}}$ is much smaller than $L_{\parallel}$.

TABLE I. Parameters used in each simulated case.

	Sc2 short	Sc2 long	Sc4 short	Sc4 long
Tilt angle (deg)	15	15	9	9
lx (m)	0.1	0.1	0.1	0.1
ly (m)	3.5	3.5	3.5	3.5
$L_{\parallel}$ (m)	2.8	2.8	2.8	2.8
T_e (eV)	10	10	20	20
T_i (eV)	20	20	60	60

Consequently $L_{\parallel}^{\text{eff}}$ in ITER is chosen much smaller than $L_{\perp}$ and a reasonably value of 2.8 m has been finally introduced in simulations. This length corresponds to the toroidal width of ITER ICRF antenna and should be higher than the effective connection length. Then the radial dc potential profile should overestimate the radial broadening due to rf transverse currents.

VI. RECTIFIED POTENTIAL SIMULATION APPLIED TO ITER ICRF ANTENNA

SEM code was used to compute from rf potentials the dc rectified potential to evaluate the new shape of the potential structures in front of the antenna design presently envisaged for ITER ICRF launcher (April 2007 design). The rf potential map is obtained from integration of the parallel electric field of the slow wave along an open magnetic line. Moreover, the electric field map have been computed by TOPICA code able to solve a 3D electric field in front of the ICRF antenna.[20] The plasma simulated is a deuterium plasma for simplification (obviously ITER plasma is a mixture of 50% of deuterium and 50% of tritium) and the parameters used

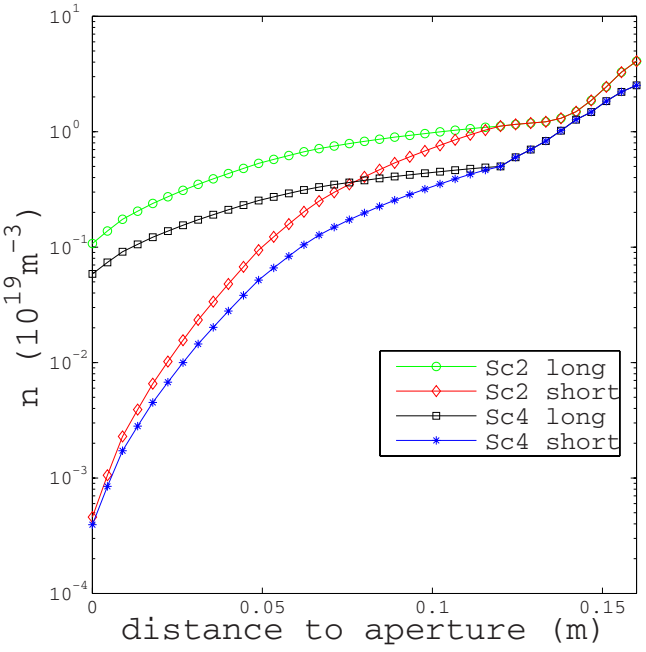

FIG. 10. (Color online) Density profile for each scenario.

appeared in Table I for each scenario. *lx* and *ly* are the radial width and the poloidal height of the simulated box. The combination of each varying parameter gives 12 scenarios: 9° or 15° degrees for the tilt angle associated to $T_e = 10$ and 20 eV, respectively, different density profiles for short and long SOL (Fig. 10); thus conditioning the skin depth of the slow wave and three phasings for the four straps antenna.

rf and dc rectified maps can be compared in Figs. 11(a)

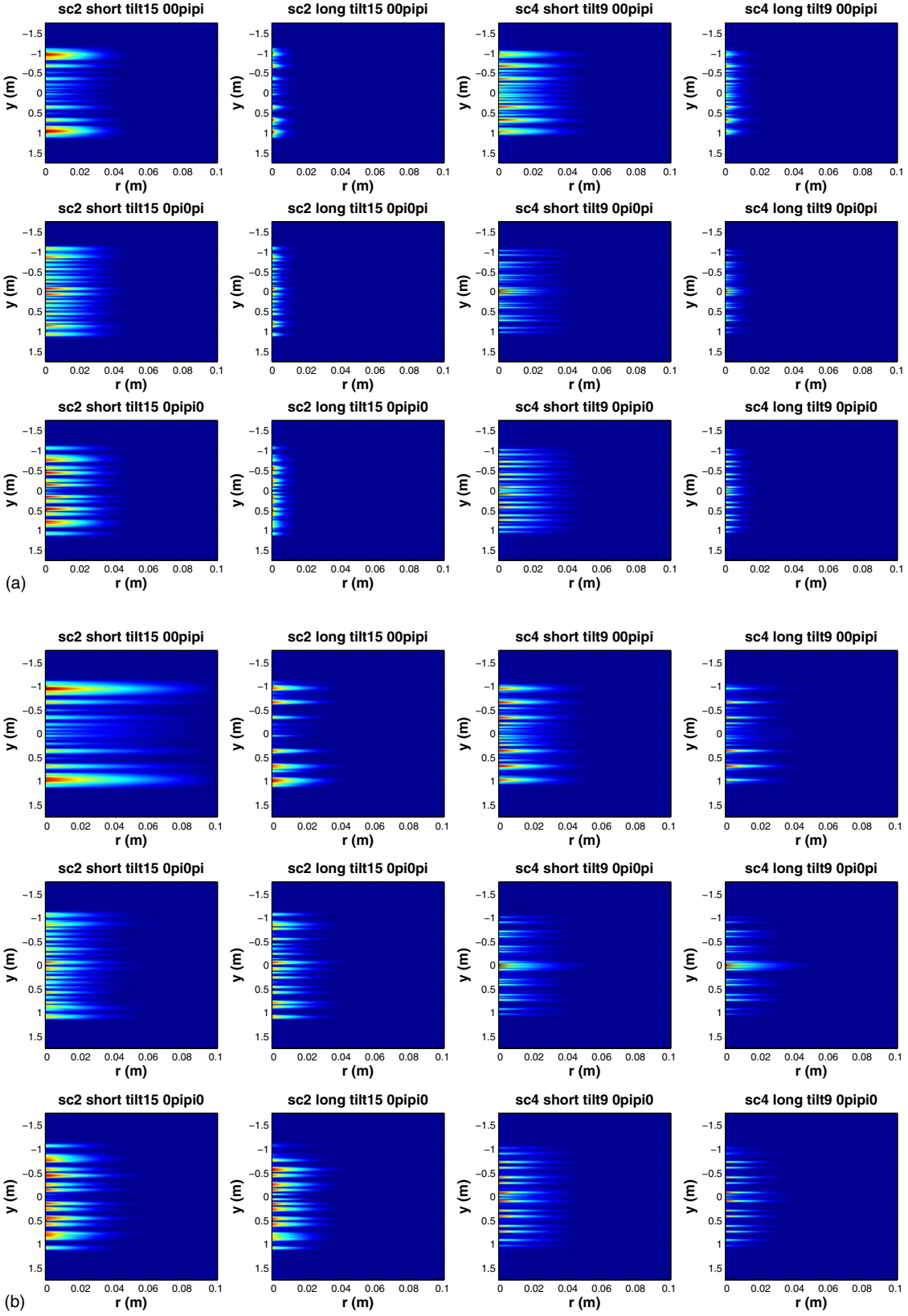

FIG. 11. (Color online) Poloidal potential map in front of ICRF ITER-like antenna. (a) rf potential as a function of *y* (poloidal direction) and *r* (radial direction). (b) dc rectified potential as a function of *y* (poloidal direction) and *r* (radial direction).

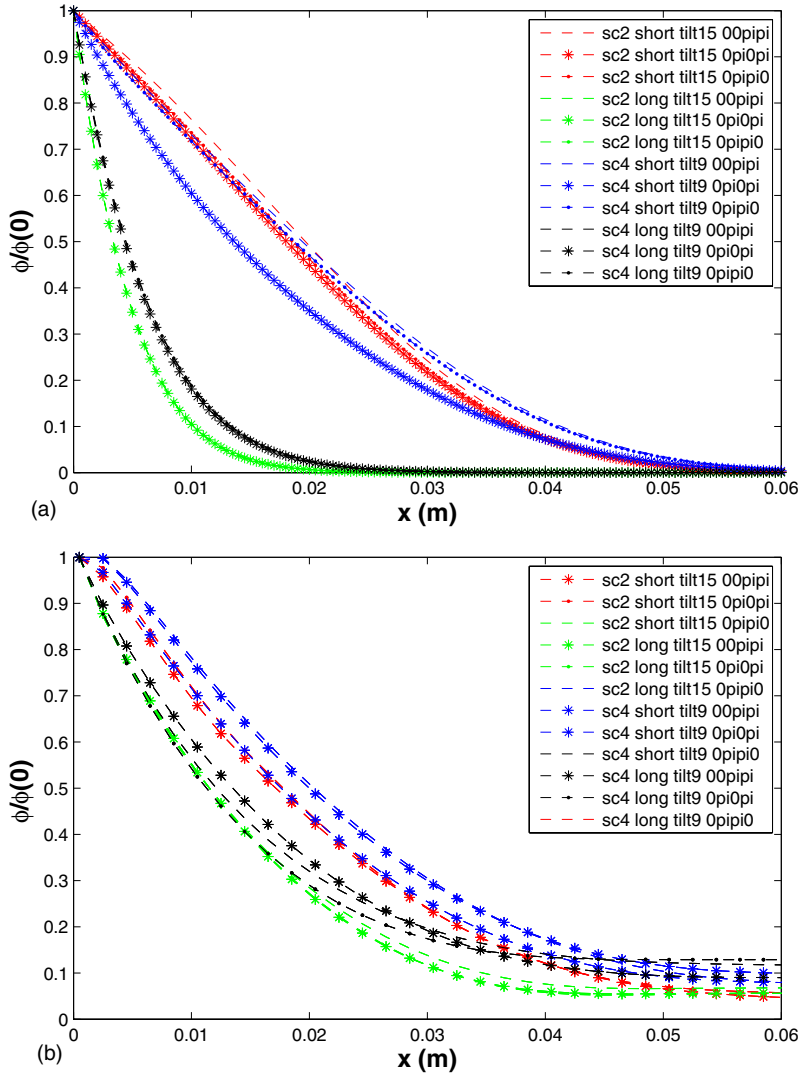

FIG. 12. (Color online) Characteristic decreasing lengths for 12 ITER antenna scenarios as a function of x equivalent to the radial direction in a Tokamak. ϕ_{rf} is the rf potential profile and ϕ is the rectified dc potential profile.

and 11(b), respectively. The main difference appears for long SOL scenarios for which the penetration length is widely increased in the rectified potential maps. The average potential along the poloidal direction gives the potential profile along x, which corresponds to radial direction in the tokamak.

These rf and rectified profiles are drawn in Figs. 12(a) and 12(b). The first one shows two decreasing scales, the shorter one corresponds to long SOL scenarios and the longer to the short SOL scenarios according to density profiles given in Fig. 10. The Fig. 12(b) makes appear only one decreasing scale because, according to the theory given by Eq. (23) the decreasing length tends to L the characteristic length for perpendicular rf currents because here x_0 the rf decreasing length is two times smaller than L. Table II and Fig. 13 summarize the values of x_0, L_0, L_{nl}, and L for each scenario.

The theoretical value L calculated from Eq. (7) is clearly close to the simulated value L_{nl} and L_0 is always higher than

TABLE II. The lengths x_0 the typical width of the rf structure, L_{nl} the computed width along which rf currents propagate, and L the theoretical width corresponding to these same currents are compared for 12 different scenarios applied to ICRF ITER antenna.

Scenario	SOL	Phasing	x_0	L_{nl}	L [Eq. (30)]
Sc2	Short	00pipi	24.5	22.5	18.4
Sc2	Short	0pi0pi	23	20.5	18.4
Sc2	Short	0pipi0	23.5	20.5	18.4
Sc4	Short	00pipi	25	22.5	23.5
Sc4	Short	0pi0pi	19	20.5	23.5
Sc4	Short	0pipi0	24.5	22.5	23.5
Sc2	Long	00pipi	4.5	14.5	18.4
Sc2	Long	0pi0pi	4.5	14.5	18.4
Sc2	Long	0pipi0	4.5	14.5	18.4
Sc4	Long	00pipi	6	12.5	23.5
Sc4	Long	0pi0pi	6	14.5	23.5
Sc4	Long	0pipi0	6	12.5	23.5

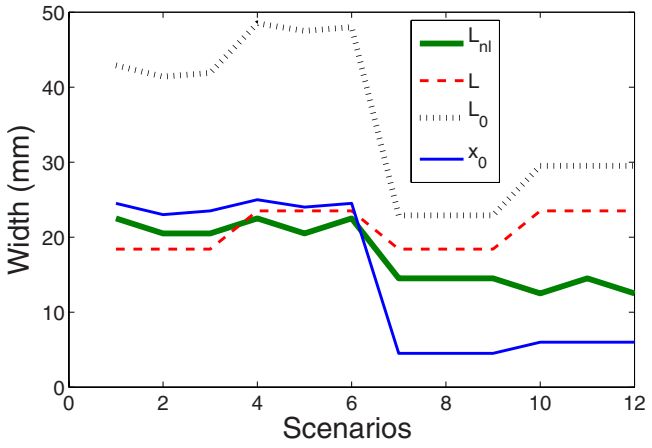

FIG. 13. (Color online) Comparison of the width L_{nl} with x_0 and L with respect to the 12 simulated scenarios.

L_{nl} which seems to depend on x_0 as it is defined in L_0. This length L_0 can then be chosen as a good upper bound to estimate the transverse broadening of the dc potential structures in tokamak SOL.

VII. CONCLUSION

The fluid modeling of a flux tube ended by rf sheaths and able to exchange rf currents transversally allows to calculate the dc rectified potentials located in the tokamak SOL for example. As the time analysis of the model had already been completed in another paper,[7] here we study specifically the spatial broadening of rectified potential structures in the radial direction (perpendicular to the magnetic field). The spatial linearization of the model gives the characteristic transverse length L along which rf transverse current effects occur. This can be seen as a broadening length or a penetration length in the edge plasma. Only rf current term is taken into account in the present paper because this is the largest current term in the plasma in front ICRF antennas. The linear theory predicts that the width of dc potential structures is of the order of x_0 the skin depth for the slow wave when $L \ll x_0$ and of the order of L as soon as $L \gg x_0$.

The validity of this linear length is confirmed by simulations run in SEM code able to take into account the nonlinearity of the model and to compute self-consistently rf potentials and rf currents. We deduce that the computed nonlinear length L_{nl} is of the order of $L(\omega)$ and smaller than $L_0 = x_0 + \sqrt{L_{\|}\rho_{ci}/2}$, then $L(\omega)$ or simply L_0 are good approximations to evaluate the transverse penetration of dc rectified potential structures in a magnetized rf plasma. For typical fusion edge plasmas, L is centimetric or more and thus higher than x_0. The size of dc potential structures in front of ICRF antennae should be close to L which can be easily calculated by knowing the magnetic connection length, the Larmor radius, the rf frequency and the ion cyclotron frequency.

However, the flute hypotheses is not valid for parallel connection length higher than 56 cm according to an electrostatic wave model including sheaths[14] with typical edge tokamak plasma parameters. Thus transverse rf currents might be only exchanged over a fraction of magnetic connection length, which means an effective parallel length $L_{\|}^{\text{eff}}$. This effective length $L_{\|}^{\text{eff}}$ has been deduced from $L_{\perp}$ measured by probes[9] and gives 0.35 m in Tore Supra, which confirms that $L_{\|}$ has to be replaced by $L_{\|}^{\text{eff}}$ in the model to not overestimate the broadening of dc potential structures.

This model was applied to an ITER plasma in front of a typical ITER-like ICRF antenna with $L_{\|}^{\text{eff}} = 2.8$ m. Moreover, the result is that the typical width of these structures is close to L when it is longer than x_0 the length of the initial rf structure. On the contrary, when L is smaller than x_0 the dc rectified structure is not broadened as predicted in linear modeling.

The main conclusion concerning this work is that the potential dc structure in front of ICRF antennas in tokamaks and next in ITER does not penetrate deeply in the plasma so that they should not reach the separatrix. The corollary of this dc structure is that they can propagate far away from their starting point along the magnetic field to bias remote regions of the SOL and then induce convective cells. From the finite effective length found here which is smaller than the magnetic connection length in tokamak SOL we deduce that parallel potential gradients exist, which means that rf and inertia currents[21,16] can be important in the edge plasma.

Nevertheless, the length $L_{\|}^{\text{eff}}$ is calculated here supposing that $L_{\perp}$ is centimetric, which supposes to already know the perpendicular width of potential structures. In future works, $L_{\|}^{\text{eff}}$ should be evaluated with a 2D full electromagnetic model with self-consistent boundary conditions.

[1] L. Colas, A. Ekedahl, M. Goniche, J. P. Gunn, B. Nold, Y. Corre, V. Bobkov, R. Dux, F. Braun, J.-M. Noterdaeme, M.-L. Mayoral, K. Kirov, J. Mailloux, S. Heuraux, E. Faudot, J. Ongena, and ASDEX Upgrade Team JET-EFDA Contributors, Plasma Phys. Controlled Fusion **49**, B35 (2007).
[2] L. Colas, S. Heuraux, S. Bremond, and G. Bosia, Nucl. Fusion **45**, 767 (2005).
[3] J.-M. Noterdaeme and G. Van Oost, Plasma Phys. Controlled Fusion **35**, 1481 (1993).
[4] V. A. Godyak and A. A. Kuzovnikov, Fiz. Plazmy **1**, 496 (1975).
[5] M. A. Lieberman, IEEE Trans. Plasma Sci. **16**, 638 (1988).
[6] M. A. Lieberman, IEEE Trans. Plasma Sci. **17**, 338 (1989).
[7] E. Faudot, L. Colas, and S. Heuraux, Phys. Plasmas **13**, 042512 (2006).
[8] R. Van Nieuwenhove and G. Van Oost, Plasma Phys. Controlled Fusion **34**, 525 (1992).
[9] J. P. Gunn, L. Colas, A. Ekedahl, E. Faudot, V. Fuchs, S. Heuraux, M. Goniche, M. Koèan, A. Mendes, A. Ngadjeu, V. Petržílka, F. Saint-Laurent, and K. Vulliez, Proc. 22nd IAEA Fusion Energy Conference, Geneva 2008 EX/P6–32.
[10] D. A. D'Ippolito and J. R. Myra, Phys. Plasmas **7**, 3301 (2000).
[11] D. A. D'Ippolito, J. R. Myra, J. Jacquinot, and M. Bures, Phys. Fluids **10**, 3603 (1993).
[12] L. Colas, D. Milanesio, E. Faudot, M. Goniche, and A. Loarte, J. Nucl. Mater. **390–391**, 959 (2009).
[13] A. V. Nedospasov and D. A. Uzdensky, Contrib. Plasma Phys. **34**, 478 (1994).
[14] D. A. D'Ippolito and J. R. Myra, Phys. Plasmas **13**, 102508 (2006).
[15] D. A. D'Ippolito and J. R. Myra, Phys. Plasmas **16**, 022506 (2009).
[16] V. A. Rozhansky, A. A. Ushakov, and S. P. Voskoboinikov, Plasma Phys. Rep. **24**, 777 (1998).
[17] A. Carlson, Phys. Plasmas **8**, 4732 (2001).
[18] M. Becoulet, L. Colas, S. Pécoul, J. Gunn, Ph. Ghendrih, A. Bécoulet, and S. Heuraux, Phys. Plasmas **9**, 2619 (2002).
[19] E. Faudot, S. Heuraux, and L. Colas, AIP Conf. Proc. **933**, 219 (2007).
[20] D. Milanesio, V. Lancellotti, L. Colas, R. Maggiora, V. Kyrytsya, and G. Vecchi, Plasma Phys. Controlled Fusion **49**, 405 (2007).
[21] V. A. Rozhansky, S. P. Voskoboynikov, E. G. Kaveeva, D. P. Coster, and R. Schneider, Nucl. Fusion **41**, 387 (2001).